Materials Transactions, Vol. 57, No. 10 (2016) pp. 1691 to 1697

Enhanced Ductility of *In Situ* Synthesized (TiB+La_2O_3)/IMI834 Composite by TRIPLEX Heat Treatment

Jiuxiao Li, Yuanfei Han, Liqiang Wang, Liangyu Chen and Weijie Lu*

State Key Laboratory of Metal Matrix Composites, Shanghai Jiao Tong University, Shanghai 200240, China

The effects of a new TRIPLEX heat treatment on the microstructure and the mechanical properties of *in situ* synthesized (TiB+La_2O_3)/IMI834 composite (TMCs) were studied. The microstructures and the morphology of reinforcements after heat treatment were characterized by optical microscopy, scanning electron microscopy (SEM), electron backscattered diffraction (EBSD) and transmission electron microscopy (TEM). The martensite variation was *in situ* observed in the processing of TRIPLEX heat treatment by confocal laser scanning microscope (CLSM). The results showed that the microstructure of specimens after TRIPLEX heat treatment exhibits laminar structure with high aspect ratio. The percent of low angle boundaries of TMCs treated by TRIPLEX heat treatment and β heat treatment is about 22.71% and 25.32%, respectively. Compared with β heat treatment, the ductility of titanium matrix composites after TRIPLEX heat treatment was improved significantly. Tiny perpendicular cracks on TiB reinforcement and the crack initiating in matrix were *in situ* observed at the same time by CLSM during tensile test. [doi:10.2320/matertrans.M2015268]

(Received July 2, 2015; Accepted January 7, 2016; Published September 25, 2016)

Keywords: *titanium matrix composite, reinforcements, heat treatment, microstructure, tensile properties*

1. Introduction

The particulate/whiskers reinforced titanium matrix composites (TMCs) have drawn special attentions for their excellent and balanced properties, such as lower costs, isotropic properties, high specific strength, specific stiffness and high fracture resistance. As a consequence, TMCs are widely used in aerospace, advanced weapon systems and the automotive industry.[1,2] The selection of matrix and reinforcement of TMCs would generally influence the manufacturing processing, microstructure development and therefore the final mechanical performances. In practice, the reinforcements are expected to have high thermal stability, similar density and thermal expansion coefficients with those of the matrix. Moreover, its elasticity modulus is required to be much higher than that of the matrix. As has been reported, the fibers or particles (such as SiC, TiC, TiB, TiB_2, B_4C, TiN or Al_2O_3) are usually adopted in TMCs as reinforcements.[3,4] The properties of TMCs depends highly on the factors including matrix microstructure, nature, type, size, morphology and volume fraction of reinforcements, as well as the interfacial structures between matrix and reinforcements.[5]

With the material of both matrix and reinforcement determined, proper heat treatment could improve the mechanical properties of TMCs by altering the overall microstructure. Conventional candidates for heat treatment of Ti alloys are β heat treatment (βHT) and $\alpha+\beta$ heat treatment ($\alpha+\beta$HT). Greater creep property of TMCs is achieved by βHT at the cost of ductility. On the contrary, TMCs treated by $\alpha+\beta$HT present greater ductility but poor creep properties.[6] In recent years, Ti alloy are treated frequently by TRIPLEX heat treatment (β_3HT) method.[7–9] TMCs after β_3HT have a good combination of properties such as tensile, creep properties and fracture toughness.[5,6,10] But the detail analysis of microstructure morphology and underlying fracture mechanism of TiB still remain unclear.

The purpose of the present work is to investigate phase change, microstructure morphology change in process of TRIPLEX heat treatment by EBSD and confocal laser scanning microscope (CLSM). TiB reinforcement fracture is *in situ* observed by CLSM, and further discussed in this paper.

2. Experimental Procedure

The (TiB+La_2O_3)/Ti composites in the current study were prepared by *in situ* synthesized technique in a consumable vacuum arc-remelting furnace. Compared with traditional preparation techniques of TMCs, *in situ* synthesized technique overcomes the problems of pollution reinforcements and the wettability between reinforcements and matrix.[11,12] The matrix alloy is the near-alpha high temperature titanium alloy IMI834. The reinforcements TiB (whiskers) and La_2O_3 (particles) are obtained via internal reaction taken place in the melts:

$$12Ti + 2LaB_6 + 3[O] = 12TiB + La_2O_3 \quad (1)$$

Supposing that the weight of LaB_6 is x in eq. (1)

$$W_{TiB} = \frac{12 \times MW_{TiB}}{2 \times MW_{LaB_6}} x \quad (2)$$

$$W_{La_2O_3} = \frac{MW_{La_2O_3}}{2 \times MW_{LaB_6}} x \quad (3)$$

$$V_{TiB} = W_{TiB}/\rho_{TiB} \quad (4)$$

$$V_{La_2O_3} = W_{La_2O_3}/\rho_{La_2O_3} \quad (5)$$

$$TiB_{(\text{volume fraction})} = \frac{V_{TiB}}{V_{TiB} + V_{La_2O_3} + V_{matrix}} \times 100\% \quad (6)$$

$$La_2O_{3(\text{volume fraction})} = \frac{V_{La_2O_3}}{V_{TiB} + V_{La_2O_3} + V_{matrix}} \times 100\% \quad (7)$$

Where MW is the molecular weight, W is weight and V is volume. Substituting eq. (2), (3), (4), (5) into eq. (6), the volume fraction of TiB 1.82% can be obtained by eq. (6). Substituting eq. (2), (3), (4), (5) into eq. (7), the volume fraction of La_2O_3 0.58% can be obtained by eq. (7). The

*Corresponding author, E-mail: luweijie@sjtu.edu.cn

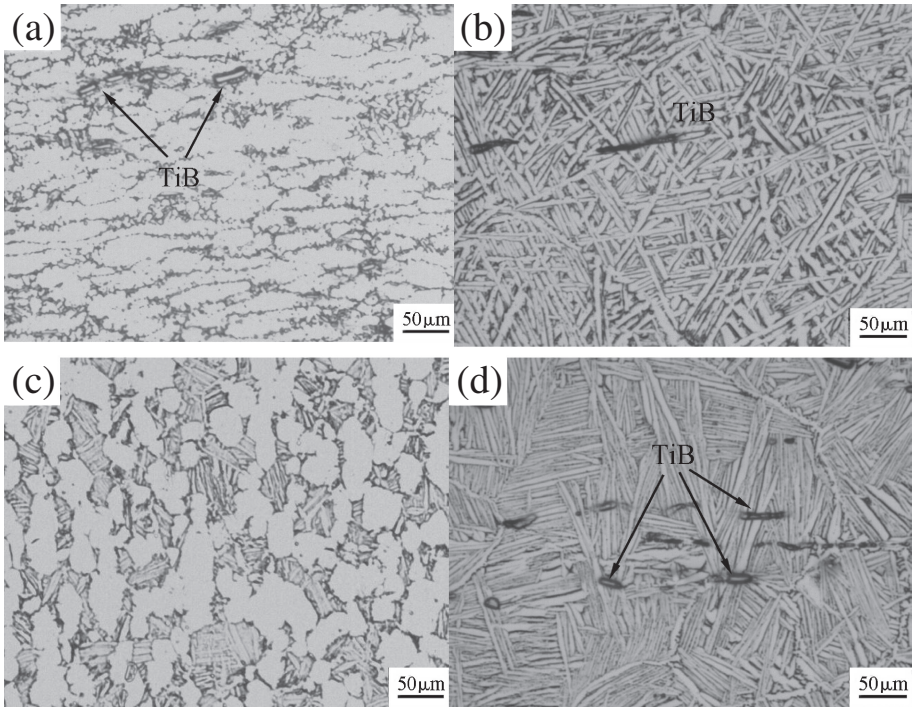

Fig. 1 Microstructure of TMCs (a) before heat treatment, (b) after β_3 HT, (c) after $\alpha+\beta$ HT, (d) after β HT.

Table 1 The heat treatment methods of TMCs.

Heat treatment methods	β phase area	$\alpha+\beta$ phase area	
$\alpha+\beta$	—	1263 K/2 h, AC	923 K/4 h, AC
β	1333 K, 1 h + AC	—	923 K/4 h + AC
TRIPLEX (β_3)	1333 K, 1 h + OQ	1253 K/1.5 h + AC	923 K/4 h + AC

Heat treatment: HT; β_3 HT: TRIPLEX heat treatment; AC: air cooling; WQ: water quenching; OQ: oil quenching.

ingots were hot-forged into a diameter of Φ70 mm rods. The beta transformation temperature of TMCs was evaluated by microstructure methods. The microstructures of TMCs were observed every increase of 5 K at the beta transformation temperature of IMI 834, until the α phases were not observed in microstructures photo. This temperature is the beta transformation temperature of TMCs. The beta transformation temperature of TMCs is approximately 1313 K. The heat treatment methods of TMCs are listed in Table 1.

Microstructure were examined by optical microscope (OM), JSM-6700F scanning electron microscope (SEM), EBSD and Philips-CM 200 transmission electron microscopy (TEM).

The phase transition of TMCs was *in situ* observed by CLSM in the process of heat treatment. The heating rate is 573 K/s, then cooled at 288 K/s. The fracture mechanism of TMCs treated by β_3 HT in the process of tensile at 923 K was also observed by CLSM. The gauge sections of the tensile specimens are 20 mm × 1 mm × 3 mm. A little notch is prepared in middle of tensile specimens. The strain rate is $10^{-3}\,s^{-1}$.

The gauge sections of the tensile specimens are 15 mm × 4 mm × 1.5 mm. Room temperature tensile tests were carried out using Zwick T1-Fr020TN materials testing machine. High temperature tensile tests were carried out by using CSS-3905 testing machine at 873 K, 923 K and 973 K. The strain rate is $10^{-3}\,s^{-1}$ at both room temperature and high temperature.

3. Results and Discussion

3.1 Microstructure of TMCs after heat treatment

Figure 1 shows the microstructure of initial TMCs (Fig. 1(a)) and those after three heat treatment methods (Fig. 1(b)–(d)), i.e., β_3 HT, $\alpha+\beta$ HT and β HT, respectively. The microstructure of TMCs treated by β_3 HT is laminar structure. $\alpha+\beta$ HT is bimodal structure and β HT is widmanstätten structure. As can be seen by comparing Fig. 1(b) and (c), the width of $\alpha+\beta$ colony after β_3 HT is smaller than that of β HT, while the α laminar in a single colony after β HT exhibit a much thinner morphology than that of β_3 HT. TiB whiskers in TMCs show good alignment along the forging direction.

Figure 2(a) shows EBSD microscopy of TMCs after β_3 HT. The microstructure of specimens after β_3 HT is laminar structure. The $\alpha+\beta$ colonies consist of α laminar of nearly the same orientation (represented by the same color), which has the largest aspect ratio. Few of big strong $\alpha+\beta$ colonies are observed in Fig. 2(a). The densities of $[0001]\alpha$, $[2\bar{1}\bar{1}0]\alpha$ and $[10\bar{1}0]\alpha$ in Fig. 2(a), as illustrated by colors in Fig. 2(d), indicate that α phase with different orientations are uniformly distributed. Figure 2(b) shows EBSD microscopy of TMCs after β HT. The microstructure of specimens after β HT is widmanstätten structure that consists of larger $\alpha+\beta$ colonies, as that represented by big different color pieces. The width of $\alpha+\beta$ colony of orientations $[2\bar{1}\bar{1}0]\alpha$ is less than those of [0001] and $[10\bar{1}0]$. Figure 2(c) shows the

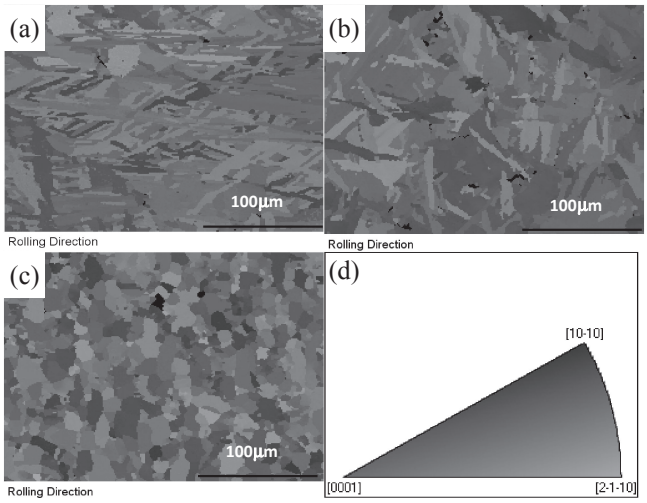

Fig. 2 EBSD microscopy of TMCs after heat treatment (a) β_3 HT (b) βHT (c) $\alpha+\beta$HT.

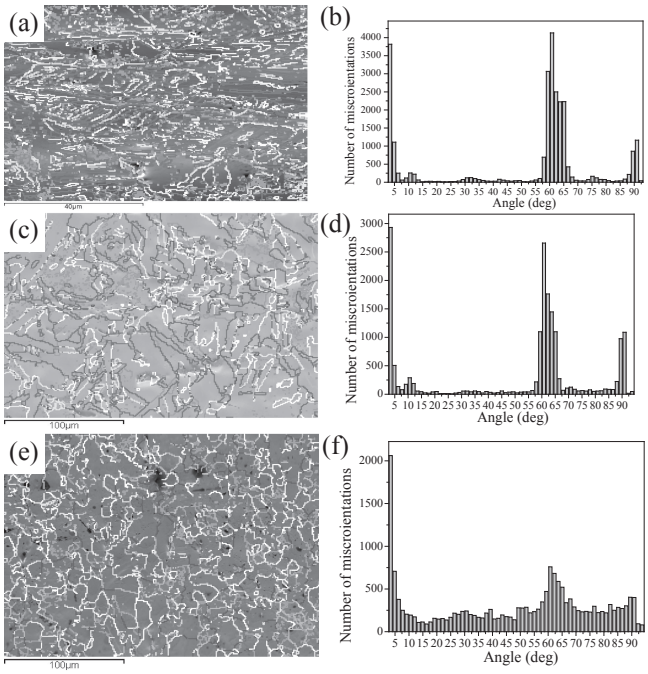

Fig. 3 Misorientation of TMCs after heat treatment: (a) β_3 HT (b) number of misorientation of β_3 HT (c) βHT (d) number of misorientation of βHT (e) $\alpha+\beta$HT (f) number of misorientation of $\alpha+\beta$HT.

EBSD microscopy of TMCs after $\alpha+\beta$ heat treatment. A typical bimodal structure is observed, with primary α phase distributed on $\alpha+\beta$ colonies. The orientation between α laminar and α laminar is similar in $\alpha+\beta$ colony. Therefore, EBSD microscopy of TMCs after $\alpha+\beta$HT obtained equiaxed microstructure.

Figure 3 shows misorientations of TMCs after heat treatment. The colored lines display the misorientation angles (θ) between neighboring pixels. The green lines correspond to the low angle boundaries ($2 < \theta < 17°$), the cyan ones to the high angle boundaries ($17 < \theta < 32°$), other colors ones to the $\theta > 32°$ high angle boundaries. A lot of low angle boundaries are surrounded by the high angle boundaries. Low angle boundaries are mainly the grain boundaries between α/α lamella in within $\alpha+\beta$ colony, while the high angle boundaries are the boundaries between primary α grains and primary α grains, between primary α grains and $\alpha+\beta$ colony or between $\alpha+\beta$ colony and $\alpha+\beta$ colony. The percent of low angle boundaries of TMCs treated by β_3 HT, βHT, $\alpha+\beta$HT are about 22.71%, 25.32% and 21.54%, respectively.

A statistical analysis on the grain sizes of TMCs after heat treatment is carried out in Fig. 4. Grain size of TMCs after β_3 HT or βHT is observed in Fig. 4(a), (b), respectively. Previous result (Fig. 3(a), (b)) shows that both of the specimens after βHT and β_3 HT are consisted of $\alpha+\beta$ colony. However, the grain size of TMCs after β_3 HT is much smaller compared with that of TMCs after βHT. The grain size of TMCs after $\alpha+\beta$HT is distributed more homogeneously as can be seen in Fig. 4(c).

The TRIPLEX heat treatment (β_3 HT) consists of three procedures: β solution, $\alpha+\beta$ anneal, and aging. Specifically, the first step involves β solution heat treatment at 1333 K then oil quenched to room temperature. This procedure leads to the phase transformation of $\beta \rightarrow \alpha'$, which is due to the fast cooling rate after β solution. The TEM microscopy of TMCs treated by the first step of β_3 HT is high aspect ratio martensite, as shown in Fig. 5(a). In the second step of β_3 HT, the specimens are annealed in $\alpha+\beta$ phase area and then air cooled to room temperature. The martensite started to decompose into needle-like α and β phases during this heating process. The needle-like α merged and coarsened in the process of heat preservation. The β phase, transformed to α with retained β at the grain boundaries in the process of cooling. The TEM microscopy of TMCs treated by second step of β_3 HT is laminar α in Fig. 5(b), which clearly shows that the width of α phase is nearly five times that of martensites in Fig. 5(a). During the third step, the aging of the TMCs results in the decomposition of β phase within thicker retained β phase region into the secondary fine α. However, compared with the second step of β_3 HT, the microstructure of β phases remain almost same after treated by third step of β_3 HT in Fig. 5(c). The secondary α and β phase are observed at grain boundaries in Fig. 5(d).

In order to learn more about the second step of β_3 HT process, the microstructural changes were *in situ* observed by CLSM, as illustrated in Fig. 6. Figures 6(a)–(f) shows the variation of martensite with temperature increasing from 293 K–1253 K by an average rate of 44 K/min. As temperature increases, the martensite decomposed into needle α and β. The retained α in the β grain grows and coarsen along the initial growing pathway in $\alpha+\beta$ phase region, due to a hereditary characteristic of microstructure. Few microstructural changes were observed below 873 K in Fig. 6(a), (b). The thickness of needle α increases with increasing temperature from 873 K to 1253 K, especially from 1173 K to 1253 K in Figs. 6(c)–(f). Figures 6(f), (g) witnesses a rapid variation of microstructure within 10 min at 1253 K, where the width of α increases significantly. Finally, with temperature decreasing from 1253 K to 1023 K, minor microstructural changes were observed in Fig. 6(h).

3.2 Tensile properties of TMCs after heat treatment

Table 2 lists the tensile properties of TMCs after heat

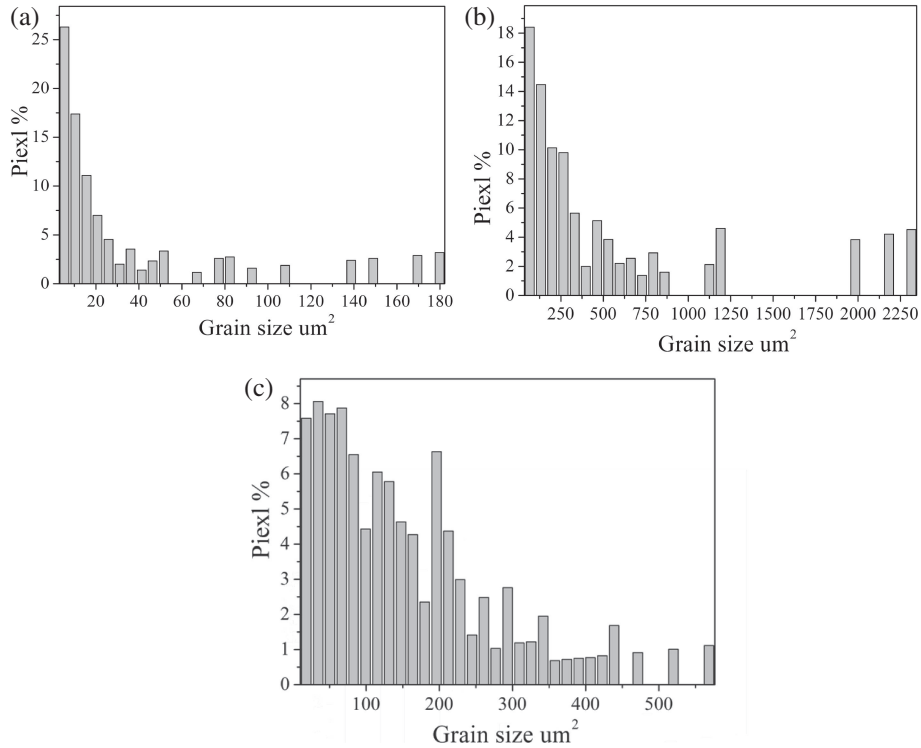

Fig. 4 Grain size of TMCs after heat treatment: (a) β_3 HT, (b) βHT, (c) $\alpha+\beta$HT.

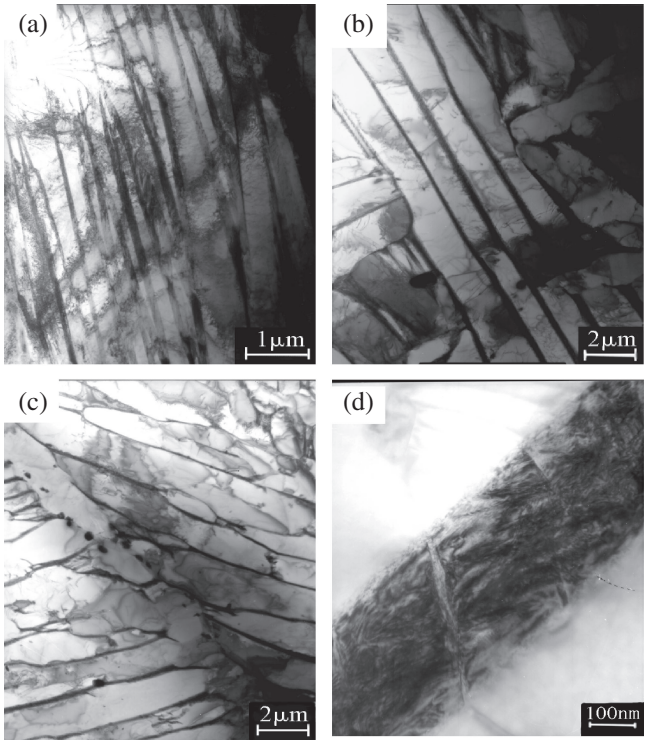

Fig. 5 TEM microscopy of β_3HT, (a) 1333 K, OQ, (b) 1333 K, OQ + 1253 K, AC, (c) 1333 K, OQ + 1253 K, AC + 923 K, AC, (d) the secondary α and β phase at grain boundaries.

Table 2 Tensile properties of TMCs after heat treatment.

Heat treatment method	Room-temperature tensile properties		High-temperature tensile properties					
			873 K		923 K		973 K	
	σ_s/MPa	δ/%	σ_b/MPa	δ/%	σ_b/MPa	δ/%	σ_b/MPa	δ/%
$\alpha+\beta$HT	1120	15.8	830	16.2	722	24	590	40.9
βHT	1180	6.5	800	13.8	756	18.6	660	27.5
β_3HT	1170	15.4	770	18.0	712	25.6	630	38.2

σ_s: yield strength; σ_b: ultimate strength; δ: the elongation of TMCs after tensile test.

treatment at room and high temperature. The yield strength of TMCs at room temperature after βHT is the highest, yet those after $\alpha+\beta$HT present the lowest value. But the elongation of TMCs after β_3HT or $\alpha+\beta$HT is enhanced by 143%, 137% respectively in comparison with that of βHT. High temperature tensile tests are carried out at 873 K, 923 K and 973 K, respectively. For each specimen, with temperature increasing, the ultimate strength of TMCs decreases, while the elongation improves correspondingly. And for specimens tested at the same temperature, TMCs treated by βHT show the highest ultimate strength at both 923 K and 973 K, while the elongations are worst. At 973 K, the ultimate strength of TMCs treated by β_3HT is reduced by approximately 4.5%, while the elongation is being enhanced by 39%, compared with those of βHT. The ultimate strength of TMCs treated by β_3HT is enhanced by approximately 6.8%, while the elongation is being reduced by 6.6%, compared with those of $\alpha+\beta$HT at 973 K.

The rate of high angle boundaries of TMCs after βHT is less than those after β_3HT. The elongation is closely related to the degree of the crack deflection. The greater the degree of crack deflection is, the better the elongation is. The high angle boundaries could effectively improve the resistance of crack propagation. The length of crack propagation with high angle boundaries rate is longer than that with low angle

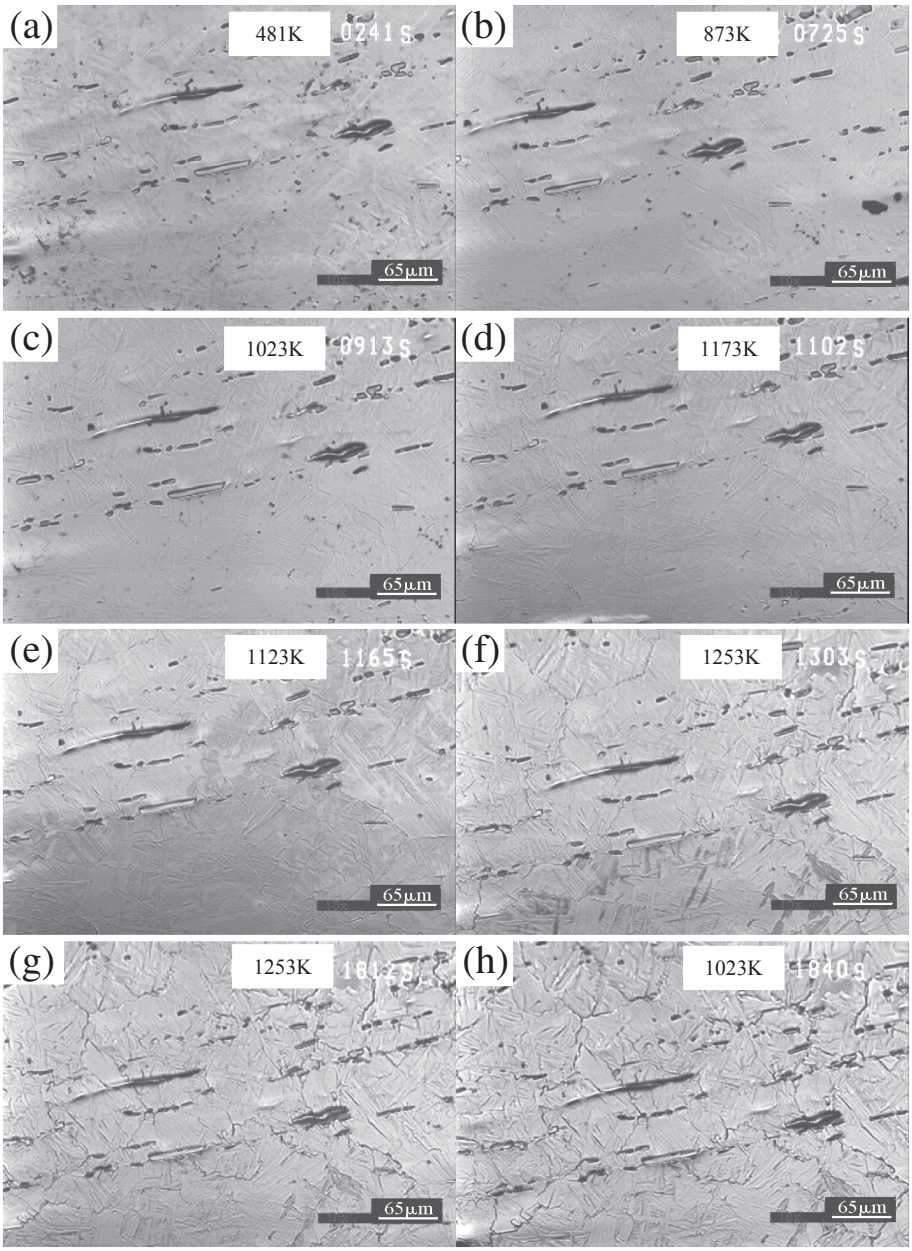

Fig. 6 The microstructural changes of martensite α': (a)~(f) heating from 481 K–1253 K, (g) retain at 1253 K for 10 min, (h) cooling 1253 K–1023 K.

boundaries rate. The elongation increases with the increase in the rate of high angle boundaries. This indicates high angle boundaries are beneficial to the ductility. This explains why the ductility of TMCs after β_3 HT increases significantly compared with that after β HT. The improvement in the strength of TMCs after β_3 HT mainly comes from the refinement of $\alpha+\beta$ colony, which reduces the sliding distance of dislocations in α phase.[13,14)]

3.3 Reinforcements

For a better understanding of the reinforcement mechanism by TiB, the microstructural evolution around TiB whisker was *in situ* observed in the tensile process by CLSM. Figure 7 shows video capture pictures of TMCs treated by β_3 HT in the process of tensile at 923 K. The stress concentration region is usually associated with the source of microcrack, since the nucleation of microcrack can release the stress. The shear ligament consists of linking the microcrack in the three-dimensional manner by shearing and the decrease of the effective stress intensity factor caused by the crack deflection.[15)] Figure 7 shows video capture pictures from 0–78 s. During the tensile test, the slip is observed within the specimen and cracks are observed around of the notch at 59 s in Fig. 7(c). With the increasing deformation, crack number increases and cracks propagate to a larger size. These cracks are probably generated on TiB reinforcements. Tiny perpendicular cracks around TiB reinforcement and the crack initiating in matrix are observed in Fig. 7(d). Cracks propagate and joined together to form a larger crack along the vertical direction of the tensile stress axial line in specimen. With the macroscopic cracks accumulated, the specimen fractures at about 80 s. Figure 8 shows a schematic diagram of the reinforcements TiB fracture mechanism. The fractures of TiB whiskers mean

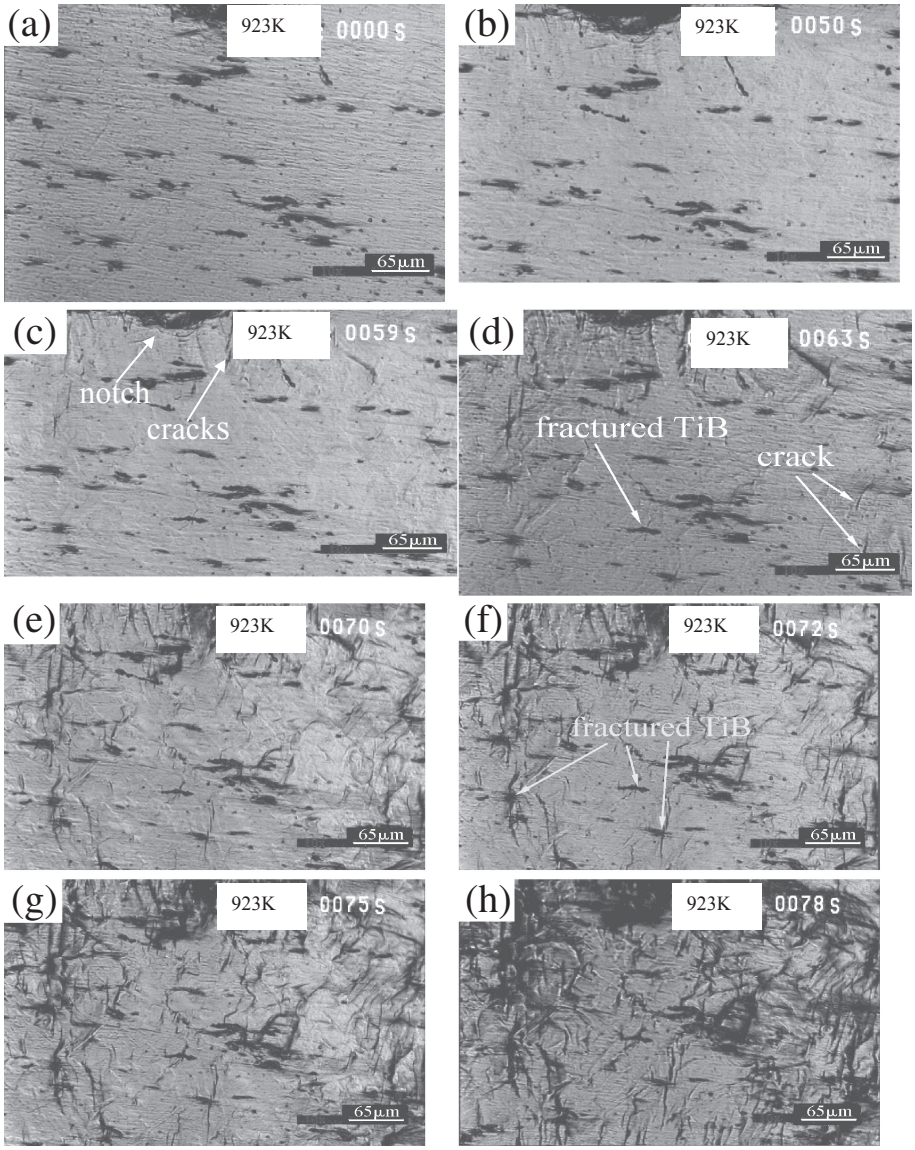

Fig. 7 Microscopy of TMCs treated by β_3 HT taken during a tensile test at 923 K, (a) 0 s, (b) 50 s, (c) 59 s, (d) 63 s, (e) 70 s, (f) 72 s, (g) 75 s, (h) 78 s.

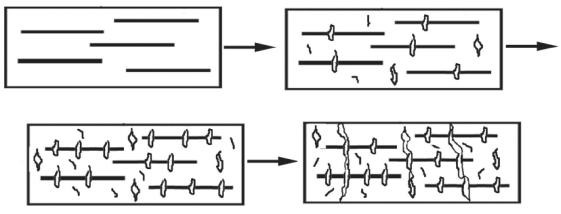

Fig. 8 Schematic diagram of the reinforcements TiB fracture mechanism.

that TiB whiskers bear tensile stress in the processing of tensile. TiB whiskers are beneficial to the strength of TMCs. With the tensile test proceeding, the matrix is being deformed before the reinforcement is fractured. Although there is a mismatch between the degrees of deformation, the strength will go through a continuous increase, which relies heavily on the interfacial bonding between matrix and reinforcement, which transferred part of stresses from matrix to TiB. Moreover, due to the interfaces, the further movement of the dislocation is hindered, resulting in the stress concentration within the interface region. Since stresses are easily concentrated and cracks are frequently observed on top of the TiB whiskers reinforcement, whiskers with larger aspect ratio will show greater degree of stress concentration. Therefore, when the deformation is small, matrix can transfer the stresses to TiB whiskers, which bear load and the strength of TMCs increases.[16] Then with the deformation increasing, the deforming stress increases, TiB whiskers fracture, crack increases on matrix and finally specimen fracture.[10]

At high temperature, the fracture mechanism of TiB whiskers is mainly determined by aspect ratio of TiB whiskers during tensile. The aspect ratio of TiB was obtained by observing 100 pieces of microstructure photos. The aspect ratio of TiB whiskers is lower than critical aspect ratio (ARc), interface between matrix and reinforcement will debond.[6,17] Nevertheless, if the aspect ratio (AR) of TiB whiskers is higher than critical aspect ratio (ARc), TiB whiskers fracture before interfacial debonding. The TiB whiskers reinforcement with higher aspect ratio bear tensile stress and improve the strength of TMCs at high temperature. The strength of

TMCs increases with increasing rate of large AR (>ARc). The critical aspect ratio (ARc) of TiB whiskers is termperature-dependent[18] and the ARc value is about 2 at room temperature, 4.4 at 873 K, 5.6 at 923 K and 7.0 at 973 K, respectively.[17]

As particle reinforcement, La can reduce the oxygen concentration. Moreover, the reinforcement of La_2O_3 can hinder the movement of the dislocation and enhance the strength of TMCs by dispersion strengthening TMCs.[6]

4. Conclusions

(1) The microstructure of TMCs after β_3 HT is laminar structure, $\alpha+\beta$ HT is bimodal structure and β HT is widmanstätten structure. The $\alpha+\beta$ colony width of TMCs after β_3 HT is thinner than that of β HT. The rate of low angle boundaries of TMCs treated by β_3 HT, β HT or $\alpha+\beta$ HT is about 22.71%, 25.32% and 21.54%, respectively.

(2) The elongation of TMCs treated by β_3 HT is enhanced greatly comparison with that by β HT, due to high rate of high grain boundaries.

(3) The cracks generated on TiB reinforcement near the tip of the whisker, where tiny perpendicular cracks are observed, and the crack initiating in matrix are observed at the same time. The TiB whiskers can improve the strength of TMCs in machanisms that depend on temperature of tensile tests.

Acknowledgements

The authors are grateful to the National Nature Science Foundation of China (Grant No: 51371114), the 973 Program under Grant No: 2012CB619600, the China Postdoctoral Science Foundation (Grant No. 2014M550235, No. 2014M561467), the Shanghai Postdoctoral Sustentation Fund (Grant No. 14R21410900) and Shanghai Academy of Spaceflight-Joint Research Centre of Shanghai Jiao Tong University advanced aerospace technology (No. US-CAST2012-14).

REFERENCES

1) H. K. S. Rahoma, Y. Y. Chen, X. P. Wang and S. L. Xiao: J. Alloy. Compd. **627** (2015) 415–422.
2) B.-J. Choi, I.-Y. Kim, Y.-Z. Lee and Y.-J. Kim: Wear. **318** (2014) 68–77.
3) V. Imayev, R. Gaisin, E. Gaisina, R. Imayev, H.-J. Fecht and F. Pyczak: Mater. Sci. Eng. A **609** (2014) 34–41.
4) M. Moradi, M. Moazeni and H. Reza Salimijazi: Vacuum. **107** (2014) 34–40.
5) J. X. Li, L. Q. Wang, J. N. Qin, Y. F. Chen, W. J. Lu and D. Zhang: Mater. Trans. **9** (2011) 1728–1733.
6) J. X. Li, L. Q. Wang, J. N. Qin, Y. F. Chen, W. J. Lu and D. Zhang: Mater. Charact. **66** (2012) 93–98.
7) X. D. Zhang, D. J. Evans, W. A. Baeslack and H. L. Fraser: Mater. Sci. Eng. A **344** (2003) 300–311.
8) H. R. Phelps, J. R. Wood, F. H. Froes and I. L. Caplan (Eds.): Titanium'92: Science and Technology, vol. 1, (1992) pp. 193–200.
9) X. D. Zhang, P. Bonniwell, H. L. Fraser, W. A. Baeslack, D. J. Evans, T. Ginter, T. Bayha and B. Cornell: Mater. Sci. Eng. A **343** (2003) 210–226.
10) J. X. Li, L. Q. Wang, J. N. Qin, Y. F. Chen, W. J. Lu and D. Zhang: Mater. Sci. Eng. A **527** (2010) 5811–5817.
11) W. J. Lu, D. Zhang, X. N. Zhang and R. J. Wu: Scr. Mater. **44** (2001) 1069–1075.
12) X. N. Zhang, W. J. Lu, D. Zhang and R. J. Wu: Scr. Mater. **41** (1999) 39–46.
13) T. S. Srivatsan, W. O. Soboyejo and R. J. Lederich: Compos. Part A **28** (1997) 365–376.
14) M. Fery and P. T. Munroe: Mater. Sci. Tech. **11** (1995) 633–641.
15) M. Niinomi and T. Kobayashi: Mater. Sci. Eng. A **213** (1996) 16–24.
16) C. J. Boehlert, S. Tamirisakandala, W. A. Curtinc and D. B. Miracled: Scr. Mater. **61** (2009) 245–248.
17) L. Xiao, W. J. Lu, J. N. Qin and D. Zhang: J. Mater. Res. **11** (2008) 3066–3074.
18) L. Xiao, W. J. Lu, Z. F. Yang, J. N. Qin, D. Zhang, M. M. Wang, F. Zhu and B. Ji: Mater. Sci. Eng. A **491** (2008) 192–198.